

Augmented heat transfer by hybrid thermosyphon assisted thermal energy storage system for electronic cooling

K Gopi Kannan, R Kamatchi*

School of Mechanical Engineering, Vellore Institute of Technology, Vellore, 632 014 Tamil Nadu, India

ARTICLE INFO

Keywords:

Thermosyphon
Thermal energy storage
Phase change material
Heat dissipation
Electronic cooling

ABSTRACT

Thermal management of electronic systems is investigated with a hybrid thermosyphon assisted thermal energy storage system. Various circulating coolants namely DI water, acetone, methanol and ethanol are used in this work. The heat input to the system varies between 50 and 90 W. Lauric acid is used as phase change material (PCM) and stored in an annular which helps to remove heat from the vapourized coolants. The molten PCM is then solidified by supplying cold water through a copper tube when the power is switched OFF. The influence of heat input on heat transfer performance such as percentage of heat removal, heat transfer coefficient (HTC) and thermal resistance of various circulating coolants is analysed. In addition, the temperature variation during the charging and discharging performance of PCM is studied by the effect of different coolants at a given heat flux. Results show that (i) the maximum percentage of heat removal and HTC of about 98.9% and 205.78 W/(m².K) are obtained for acetone at 90 W due to low boiling point, low latent heat of vapourization (LHV), low viscosity and less effect on subcooling (ii) the low thermal resistance of acetone is 0.316 K/W owing to the high vapour flow rate at maximum heat input (iii) PCM attains steady state temperature at a faster rate and the maximum thermal power absorbed is about 6.18 W when the acetone is used as a circulating coolant at 90 W.

1. Introduction

The continuous usage of microprocessor, transistors, batteries, high power density applications etc. generates a large amount of heat flux that affects its functionality. The failures in the electronic component of about 55% are mainly due to the existence of high temperature during its operation [1]. Therefore, thermal management is an imperative solution for effective performance and longevity of the devices. In recent decades, maintaining temperature stability and providing an impressive customer product is hefty challenge for thermal engineers and scientists. Although many technologies have been used in electronic gadgets, active and passive cooling plays a significant role for stable operation. In active cooling, an additional requirement of fan/blower increases power consumption and space. To mitigate this problem, researchers focus on the passive electronic cooling method.

In general, thermosyphon is the widely used technique due to its capability to remove high heat flux. In thermosyphon, the circulating coolant absorbs the heat from the evaporation section and delivers the latent heat of vapourization to the condensation section [2]. The non-dielectric liquid coolants are typically aqueous solutions which are used in electronic components owing to their excellent thermophysical properties such as high heat carrying capacity, high thermal

conductivity and low viscosity as compared with dielectric liquids [3]. Nazari et al. [4] reported that the low boiling point and dynamic viscosity of working fluids play a major role in obtaining better thermal performance and high heat transfer rate. Palm and Khodabandeh [5] numerically investigated the two-phase thermosyphon in electronic cooling using various liquid coolants. It is found that there is no specific working fluid for a thermosyphon system. Also, the various parameters such as the smaller diameter of the tube and high pressurized liquid coolant give better performance than air cooling. A thermal resistance model with closed loop thermosyphon system is experimentally analysed by Chang et al. [6]. They reported that the thermal resistance of condenser and evaporator is inversely proportional to the heat input. Chegade et al. [7] studied the thermal performance of the thermosyphon system using water as working fluid. It is observed that the optimal performance of the cooling system is obtained by governing the condenser jacket flow rate and temperature of the water. Although the effect of thermosyphon is performed in a vertical position by different research studies [8,9], there is a possible way to achieve in horizontal mode and is proved by Kwon et al. [10]. Further, the capillary pressure causes to move the liquid in the absence of gravity. Cataldo and Thome [11] developed a passive thermosyphon cooling system for removing internal heat from the power electronic device. It is suggested that the

* Corresponding author.

E-mail address: rkkamatchi@gmail.com (R. Kamatchi).

Nomenclature		V	voltage, V
A	area, m ²	<i>Greek symbols</i>	
c _p	specific heat, kJ/(kg.K)	θ	incident angle, rad
D	diameter, m	λ	wavelength, Å
h	heat transfer coefficient, W/(m ² .K)	Δ	increment
I	current, A	<i>Subscripts</i>	
k	thermal conductivity, W/(m.K)	c	convection
L	length, m	co	condensation
L _f	latent heat of fusion, kJ/kg	DI	deionized
L _v	latent heat of vapourization, kJ/kg	e	evaporation
m	mass, kg	exp	experimental
\dot{m}	mass flow rate, kg/min	HTC	heat transfer coefficient
n	integer	l	liquid
Nu	Nusselt number	LHV	latent heat of vapourization
Q	thermal power, W	PCM	phase change material
q	heat flux, W/m ²	s	solid
R	thermal resistance, K/W	t	total
T	temperature, °C		
T _α	fluid temperature, °C		
T _m	melting temperature, °C		
T _w	surface temperature, °C		

mass flow rate and thermal resistance are the two major criteria for stable operation. An arrangement of thermosyphon with vapour chamber for electronic cooling is investigated by Tsai et al. [12]. They found a decrease in thermal resistance with the rise of heat input. Furthermore, the optimum thermal performance is achieved at maximum input power. Hao et al. [13] studied the heat transfer characteristics of oscillating heat pipe charged with water, ethanol and acetone respectively. The thermal resistance is reduced by 30–63% for acetone and also has high oscillating temperature than other working fluids.

Phase change material (PCM) is the substance that changes its phase when it absorbs latent heat. A number of research studies have been reported with PCM due to its good thermal stability, small volume change and compatibility [14–16]. Walsh et al. [17] suggested that the evaporative cooling with thermal energy storage is an eco-friendly and more efficient method. Moreover, a reduction in electric power of about 2% is obtained by introducing the PCM. Weng et al. [18] experimented the heat pipe with PCM for electronic cooling. The external aid power consumption is saved to a maximum of 46% and the heat transfer rate is naturally adjusted using PCM in the cooling module. The PCM incorporated thermal control unit for a portable electronic device is experimentally and numerically analysed by Alawadhi et al. [19]. They reported that reduction in thermal induced fatigue promotes the reliable operation of the device. Fan et al. [20] investigated the PCM heat sink with internal fins in electronic cooling. The melting temperature of PCM is an important factor in protecting the device from overheating and enhances the cooling capacity of the heat sink. The thermal performance of a thermosyphon unit with RT-100 based thermal storage for probable industrial utilization is studied by Hu et al. [21]. The entire unit is virtually isothermal when the temperature is above 70 °C and the

heat transfer enhancement is not influenced by the low thermal conductivity of RT-100. The heat transfer performance of heat exchanger with latent heat storage system at different operating conditions is conducted by Diao et al. [22]. The enhancement of absorption efficiency is found as 92.5%. Also, the charging and discharging time of the PCM is decreased with an increase in the mass flow rate of the working fluid. The thermal performance of a finned coil with RT-54 is analysed by Chen et al. [23]. They revealed the HTC is directly proportional to the flow rate of working fluid during the charging and discharging process. Behi et al. [24] studied the cooling effect of PCM based heat pipe for different heat input ranging from 50 to 80 W. The cooling effect is found to be 86.7% at maximum heat input. Also, they reported the cooling effect of 11.7% is achieved by PCM alone.

The thermosyphon based fin heat sinks are quite common and numerous research work has been done since the last decade. Instead of fins, the adoption of PCM gives more amount of heat dissipation from the vapourized coolants. In addition, the extracted heat can be stored as latent heat for future usage. The hybrid thermosyphon assisted thermal energy storage system is suitable for all desired range of electronic modules to maintain optimum temperature. Therefore, it brings fool-proof thermal management to electronic gadgets in smart industries. The motivation of this work is a power-free operation that leads to less operating cost of the system.

In this study, a hybrid evaporative cooling of two-phase closed thermosyphon along with latent heat storage test facility is used to investigate the thermal performance of the electronic gadgets such as percentage of heat removal, convective HTC and thermal resistance for various circulating coolants viz. DI water, acetone, methanol and ethanol. Further, the charging and discharging capabilities of PCM are discussed in detail. Thermophysical properties of working fluids and the

Table 1
Thermophysical properties of circulating coolants at atmospheric condition (25 °C).

Properties	Measured/ Supplier data	Acetone	DI Water	Ethanol	Methanol
Boiling point T _b , °C	Supplier data	56.2 ± 0.2	99.2 ± 0.3	78.3 ± 0.4	64.7 ± 0.4
Dynamic viscosity μ _i , Pa s	Measured	0.00031 ± 0.00005	0.00088 ± 0.00001	0.00113 ± 0.00004	0.00055 ± 0.00002
Latent heat of vaporization L _v , kJ/kg	Supplier data	514.8 ± 1.5	2257 ± 3	853 ± 6	1151.6 ± 3.4
Liquid density ρ _i , kg/m ³	Measured	790 ± 9	998.5 ± 1	791 ± 8	789 ± 2.4
Specific heat c _{pi} , kJ/(kg.K)	Supplier data	2.35 ± 0.03	4.18 ± 0.01	2.40 ± 0.02	2.48 ± 0.02
Surface tension σ, N/m	Measured	0.0237 ± 0.0007	0.0728 ± 0.0007	0.0227 ± 0.0008	0.0225 ± 0.0006
Thermal conductivity k _i , W/(m.K)	Measured	0.171 ± 0.003	0.599 ± 0.003	0.172 ± 0.005	0.208 ± 0.006

characterization of PCM (lauric acid) are also studied.

2. Thermophysical properties of circulating fluids

The thermophysical properties of circulating fluids are the essential factors that affect the rate of heat transfer and hence, it is measured as a part of the present investigation. The thermophysical properties of the different circulating coolants are listed in Table 1. For ensuring the purchased product, some of the major properties are measured. The thermal conductivity (k) of the circulating fluids is measured by THW (transient hot wire) method. Therefore, a KD2 Pro thermal property analyser (accuracy: $\pm 5\%$) is used. The dynamic viscosity (μ) is found by Brookfield DV2T viscometer ($\pm 1\%$ accuracy) of the full-scale range. A bubble pressure tensiometer (Make: SITA; accuracy: $\pm 0.1\%$) is used to measure the surface tension (σ) of the circulating coolants. The density (ρ) is determined by a specific gravity bottle with an accuracy of $\pm 1\%$. The obtained values are well matched with the supplier data (Merck, India). Further, the measured thermophysical properties are compared with Dortmund Data Bank (DDB), Germany [25] and the percentage error is presented in Table 2.

3. Characterization of PCM

Lauric acid (LA, 99% pure) is used as PCM to exchange heat from the circulating coolant. Kabbara et al. [26] revealed that lauric acid undergoes a slight volume change and the degradation does not occur even after 500 cycles. Yadav and Sahoo [27] reported that lauric acid takes less time to get charging as compared with other organic PCM. The crystal arrangement of lauric acid is characterized by a Bruker, D8-Advance diffractometer with $\text{CuK}\alpha$ radiation ($\lambda = 1.54178 \text{ \AA}$), operating at $25 \text{ }^\circ\text{C}$ with a step size of 0.0142. The XRD of lauric acid (Fig. 1) exhibits the peak diffraction angles at $2\theta = 21.67^\circ$ and 24° which is indexed to the lattice plane (0 0 2) and (1 0 0) respectively. The obtained 2θ value is well matched with the existing literature [28,29]. Also, the interplanar spacing (d) is found as 4.10 \AA and 3.70 \AA using Bragg's law

$$d = \frac{0.5n\lambda}{\sin \theta} \quad (1)$$

Therefore, the observed XRD pattern indicates the crystal structure of lauric acid.

Fourier transform infrared spectroscopy (FT-IR) is used to provide the chemical stability and nature of the functional groups. The FT-IR spectrum (Make: PerkinElmer, US) is recorded over the range of $4000\text{--}500 \text{ cm}^{-1}$. Fig. 2 depicts the various functional groups present in lauric acid. It is seen that the peak at the wavenumber of 1789 cm^{-1} is induced by the carbonyl group ($\text{C}=\text{O}$). The stretching vibration of a hydroxyl group (O-H) is found at 3434 cm^{-1} . Moreover, the peaks at the wavenumber of 2915 and 2849 cm^{-1} exhibit the stretching vibrations of $-\text{CH}_3$ and $-\text{CH}_2$ groups respectively. The obtained values are in accordance with the results of Feng et al. [28] and Sari et al. [30] and hence, the purchased lauric acid is chemically stable.

The thermal stability of lauric acid is obtained by thermogravimetric analysis (TGA) using SDT Q600 analyser (Make: TA Instruments, US). It is performed over the temperature range between $25 \text{ }^\circ\text{C}$ and $400 \text{ }^\circ\text{C}$. In this study, a heating rate of $20 \text{ }^\circ\text{C}/\text{min}$ is given and the weight loss is observed until the temperature reaches $400 \text{ }^\circ\text{C}$. Fig. 3 illustrates the percentage weight loss of lauric acid with the increase of temperature. It is found that the lauric acid is consistent until $123 \text{ }^\circ\text{C}$ and the degradation starts beyond that. It is also seen that the degradation completely ends at $230 \text{ }^\circ\text{C}$ with a reduced weight of about 3.24%. Thus, it is recommended the purchased lauric acid is suitable for low/medium temperature applications.

The surface morphology of lauric acid is analysed at different magnification levels using Quanta 250 FEG scanning electron microscope (Make: Thermo Fisher FEI, US) and is shown in Fig. 4. The

crystalline nature and surface morphology of lauric acid with micropores are observed at low magnification levels (Fig. 4(a)). A formation of wrinkled morphology is seen at moderate magnification level (Fig. 4(b)). Also, a thin wavy structure of lauric acid is noticed in Fig. 4(c). Hence, the lauric acid absorbs the latent heat when it gets melted congruently due to the existence of multiple pores on the surface, substantial capillary force and absorbability.

The above characterization techniques ensure the purchased lauric acid is chemically and thermally stable and hence, it is suitable for heat transfer applications.

4. Experimental

Fig. 5 illustrates the schematic arrangement of a created test facility to investigate the internal heat removal rate from electronic gadgets. It consists of an insulated coolant tank, conical and cylindrical manifold, insulated primary PCM stored annular, heater, secondary PCM stored annular, non-return valve, voltage controller and a data acquisition system (Make: Agilent 34970A, US). The coolant tank has a size of $100 \times 100 \times 100 \text{ mm}$ with 1.2 mm in thickness. The various circulating liquid coolants such as DI water, acetone, methanol and ethanol are poured into the coolant tank and heated by coil tube immersion heater ($12 \text{ } \Omega$, 400 W). The heat input to the system varies between 50 and 90 W . The top of the coolant tank is welded with four copper tubes of 6.3 mm diameter and the other end is joined with the conical manifold. Further, the outlet of conical manifold extends through a primary PCM stored annular (diameter: 40 mm , length: 150 mm). A quantity of 168 g of PCM is used and its properties are listed in Table 3. In order to resolidify the PCM, cold water is supplied from a cold water basin and the outlet of hot water is collected by the hot water basin. The insulated components are fabricated by stainless steel and wrapped up with 6 mm thick asbestos rope to avoid heat loss. The cylindrical manifold and a secondary PCM stored annular are provided for enhancing the rate of condensation. The condensed coolant returns to the coolant tank through a non-return valve. The styrene-butadiene rubber (SBR) tubes are used for eliminating heat conduction from the coolant tank to secondary PCM stored annular. The temperature at thirteen different locations of the experimental setup is measured by T-type thermocouple (accuracy: $\pm 0.2 \text{ }^\circ\text{C}$). Although the experiments are conducted at the atmospheric conditions, it is provided with a U-tube differential manometer to ensure there is a negligible pressure drop.

The working principle is based on phase change liquid evaporative cooling. After ensuring all the connections, electrical power is given to the heater by a DC power supply. The coolant tank is filled with liquid coolant and hence, it becomes vapour. This rises to the top of the conical manifold which helps to increase the velocity of vapour flow. Then, the vapour enters into the primary PCM stored annular through the inside copper tube which extracts the heat and condenses into liquid. The circulating coolant comes again into the collecting tank due to its capillary effect. Hence, the system runs in a continuous manner without any external aid. The heat flux is set as constant until the temperature of various elements attains steady state. The PCM absorbs the heat from circulating coolant and stores as latent heat during the operating conditions. Alternately, the heater is switched OFF, the cold water is supplied to the melted primary PCM stored annular and

Table 2
Error analysis of circulating coolants.

Circulating coolants	Error in% Density (ρ)	Surface tension (σ)	Thermal conductivity (k)	Viscosity (μ)
Acetone	1.2	3.1	1.8	1.7
DI Water	0.1	1.1	0.5	1.6
Ethanol	1.1	3.5	3.0	3.4
Methanol	0.3	2.6	3.0	3.2

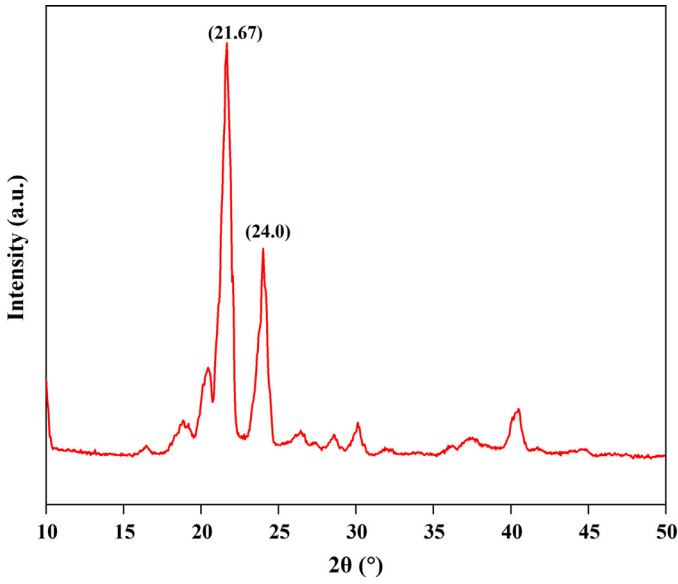


Fig. 1. X-ray diffraction pattern of lauric acid.

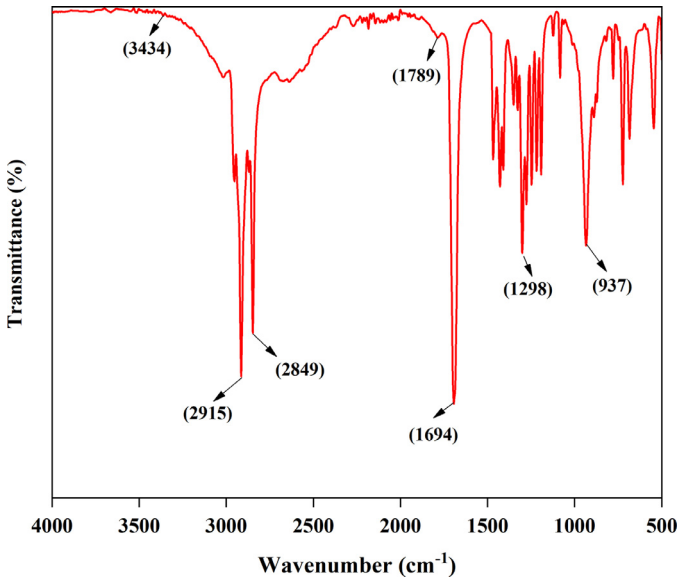


Fig. 2. FT-IR spectra of lauric acid.

absorbed latent heat which is shown in Fig. 6. The temperature of hot water at the outlet is measured for every minute by regulating the valve and this process is continued until the PCM resolidified.

The heat transfer performance of the experimental setup is estimated as

The percentage of heat removal by the circulating coolant =

$$\left(\frac{Q_s - Q_l}{Q_l} \right) \times 100 \quad (2)$$

where Q_s and Q_l are the heat supplied and convective heat loss respectively.

The convective heat loss,

$$Q_l = h_c A_c (T_w - T_\alpha) \quad (3)$$

where T_w , T_α and $h_c = \frac{Nu k}{D}$ are the surface temperature of the tube, ambient temperature and convective heat transfer coefficient respectively.

The experimental HTC (h_{exp}) is calculated by

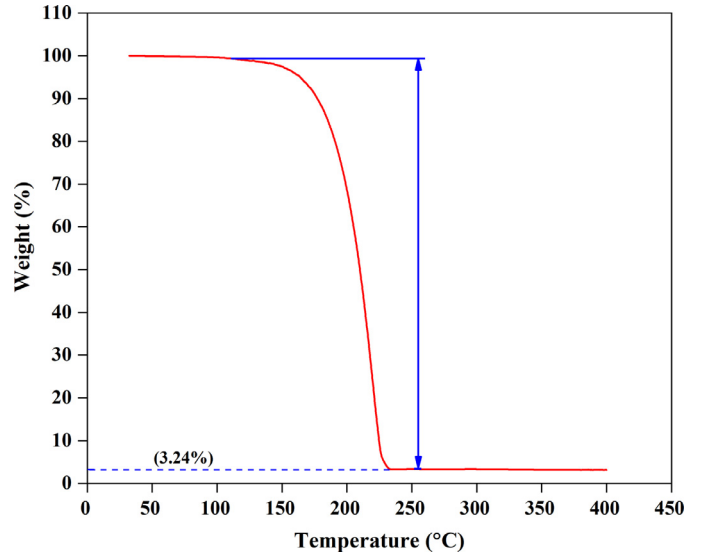


Fig. 3. Thermogravimetric analysis of lauric acid.

$$h_{exp} = \frac{q}{(T_e - T_{co})} \quad (4)$$

where T_e and T_{co} are the evaporation and condensation temperature respectively.

The effective total thermal resistance (R_t) is determined by

$$R_t = \Sigma R_e R_{co} R_c = \frac{(T_e - T_{co})}{Q_s} \quad (5)$$

where R_e , R_{co} and R_c are the thermal resistance at evaporation, condensation and convection section respectively.

The vapour flow rate of the circulating coolant (\dot{m}) is as follows

$$\dot{m} = \frac{Q_s}{L_v} \quad (6)$$

where L_v is the latent heat of vapourization of the circulating coolant.

The thermal power absorbed by the PCM is related to the mass (m), difference between initial temperature (T_i) and the final temperature (T_f) of the PCM. The total amount of stored thermal power by PCM (Q_{PCM}) is then calculated by

$$Q_{PCM} = m c_{p,s} (T_m - T_i) + m L_f + m c_{p,l} (T_f - T_m) \quad (7)$$

where L_f is the latent heat of fusion and T_m is the melting temperature of the PCM.

$$T_i = \frac{1}{4} \sum_{x=1}^4 T_{xi} \quad (8)$$

$$T_f = \frac{1}{4} \sum_{x=1}^4 T_{xf} \quad (9)$$

The measured error in length and diameter of the heater are ± 0.1 and ± 0.0001 mm respectively. The accuracy of ammeter and voltmeter are 0.25% and 0.01% respectively. The uncertainty in the heat flux, experimental HTC and the total thermal resistance are calculated using the following equations as proposed by Holmon [31] and the maximum uncertainty in the experiment is about $\pm 2.48\%$, $\pm 3.26\%$ and $\pm 3.71\%$ respectively.

$$\left(\frac{\Delta q}{q} \right)^2 = \sqrt{\left(\frac{\Delta V}{V} \right)^2 + \left(\frac{\Delta I}{I} \right)^2 + \left(\frac{\Delta L}{L} \right)^2 + \left(\frac{\Delta D}{D} \right)^2} \quad (10)$$

$$\left(\frac{\Delta h_{exp}}{h_{exp}} \right) = \sqrt{\left(\frac{\Delta q}{q} \right)^2 + \left(\frac{\Delta(\Delta T)}{\Delta T} \right)^2} \quad (11)$$

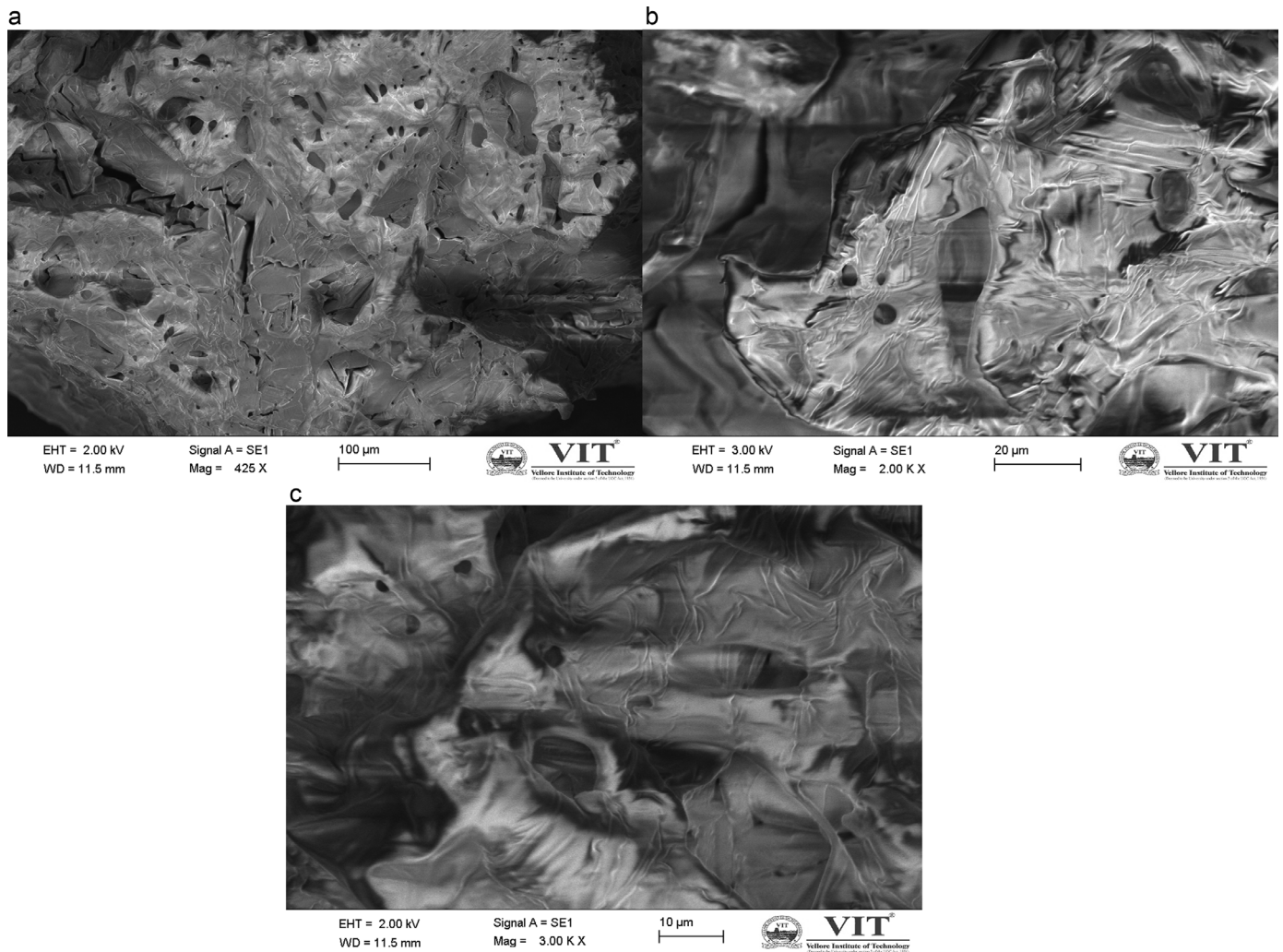


Fig. 4. SEM image of lauric acid (a) low magnification level (b) moderate magnification level (c) high magnification level.

$$\left(\frac{\Delta R_t}{R_t}\right) = \sqrt{\left(\frac{\Delta V}{V}\right)^2 + \left(\frac{\Delta I}{I}\right)^2 + \left(\frac{\Delta(\Delta T)}{T}\right)^2} \quad (12)$$

5. Results and discussion

In this study, the percentage of heat removal, HTC and thermal resistance are estimated for various circulating coolants namely DI water, acetone, methanol and ethanol. Also, the heat transfer performance of charging and discharging of stored PCM is investigated by the influence of circulating coolants.

5.1. Percentage of heat removal

Fig. 7 shows the percentage of heat removal of different circulating coolants with the heat input ranging from 50 to 90 W. As seen from Fig. 7, the percentage of heat removal is increased with the increase of heat input for all the circulating coolants. At 90 W, the heat carrying capacity of acetone, methanol, ethanol and DI water are found as 98.9%, 98.1%, 97.6% and 96.1% respectively. It is suggested that the boiling point and LHV of circulating coolant plays a major role in enhancing the percentage of heat removal. Although high LHV has more heat transferability, this is not always true and it also depends on the boiling point of the circulating coolant. It is because of the fact that the formation of vapour bubbles will be high for the low boiling point of circulating coolant [32]. Therefore, the low boiling point and low LHV

of acetone causes high vapour bubble formation which further increases the percentage of heat removal at maximum heat input.

5.2. Heat transfer coefficient

The HTC of circulating coolant depends on the geometrical aspect of the test facility, evaporation and condensation phenomenon. The experimental HTC of various circulating coolants is shown in Fig. 8. It is observed that the convective HTC increases with the supply of heat input from 50 to 90 W. Also, a maximum of 205.78 W/(m².K) is found for acetone at 90 W whereas 84.58, 119.27 and 151.80 W/(m².K) for DI water, ethanol and methanol respectively. It is suggested that the rate of evaporation of acetone is higher than the rate of condensation which leads to a high degree of superheat. The experimental investigations of Shi et al. [33] concluded that the acetone has the highest HTC value than water due to low dynamic viscosity of acetone which further causes to increase the velocity of vapour flow. Similar observations are also found by Hao et al. [13]. On the other hand, the bubble formation of the working fluid and tube diameter affects HTC to a greater extent [34]. Hence, the low dynamic viscosity and high saturation pressure of acetone increase the vapour flow rate thereby enhances the HTC.

5.3. Thermal resistance

Thermal resistance is also considered as a key factor for improving the rate of heat transfer. The cooling capacity of the circulating coolant

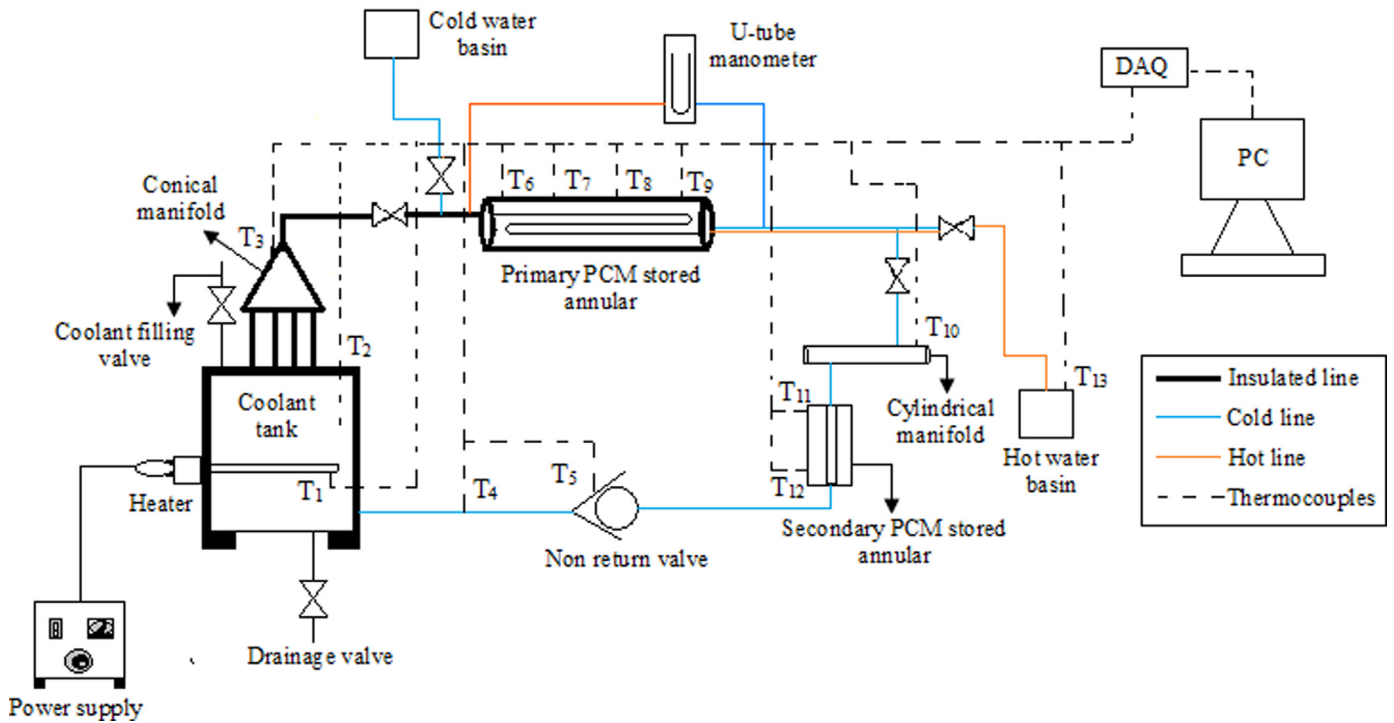


Fig. 5. An experimental setup of hybrid thermosyphon assisted thermal energy storage unit.

Table 3
Thermophysical properties of PCM.

Properties	Lauric Acid
Density ρ_s/ρ_l , kg/m ³	1004/882 ± 18
Latent heat of fusion L_f , kJ/kg	180.47 ± 5
Melting point T_m , °C	43.8 ± 1.8
Specific heat capacity $c_{p,s}/c_{p,l}$, kJ/(kg.K)	2.11/2.34 ± 0.02
Thermal conductivity k_s/k_l , W/(m.K)	0.16/0.14 ± 0.004

determines the thermal resistance of the systems. The total thermal resistance of the setup is calculated by the addition of convective resistance and thermal resistance at evaporation and condensation regions. Fig. 9 depicts the total thermal resistance of coolants for different heat inputs. It is seen that the thermal resistance of circulating coolants decreases with the increase of heat input. Also, the thermal resistance of acetone at 90 W is found as 0.316 K/W while 0.768, 0.544 and 0.428 K/W for DI water, ethanol and methanol respectively. The high vapour flow rate inside the condensation region may be the reason for low

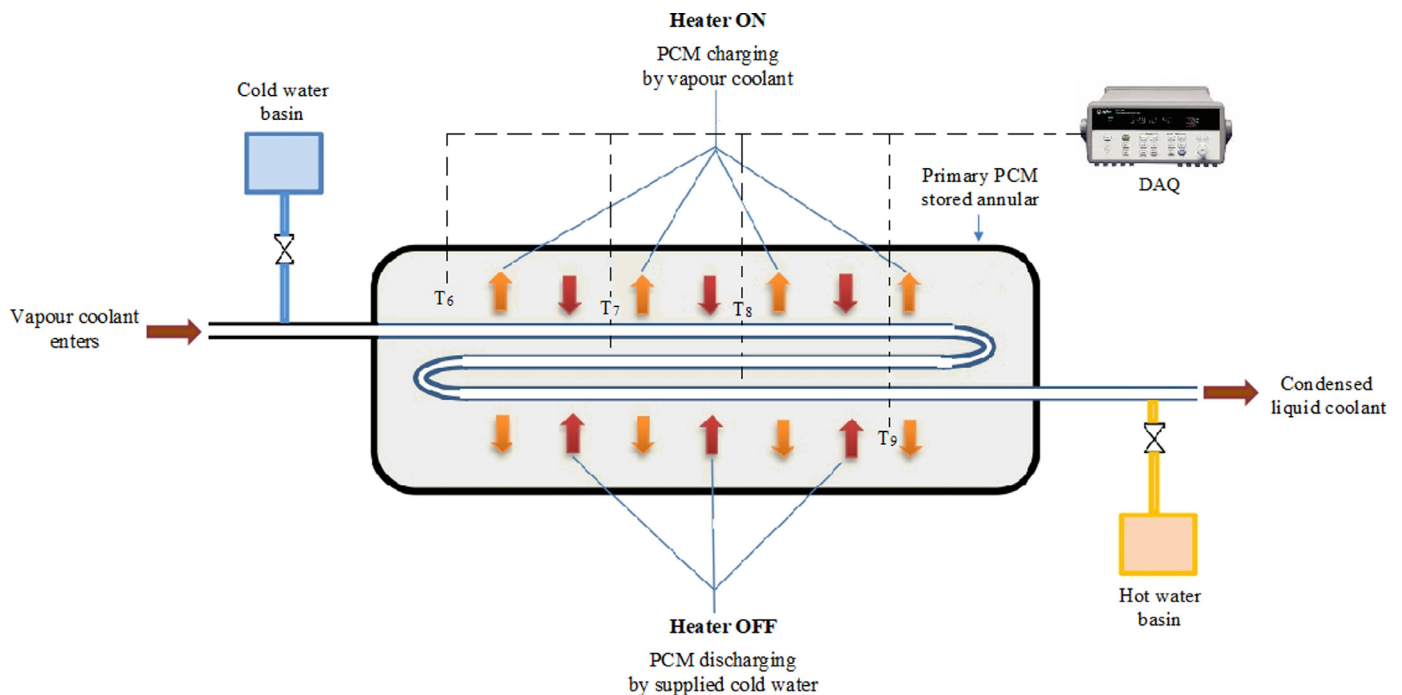


Fig. 6. Schematic view of primary PCM stored annular with the different position of thermocouples.

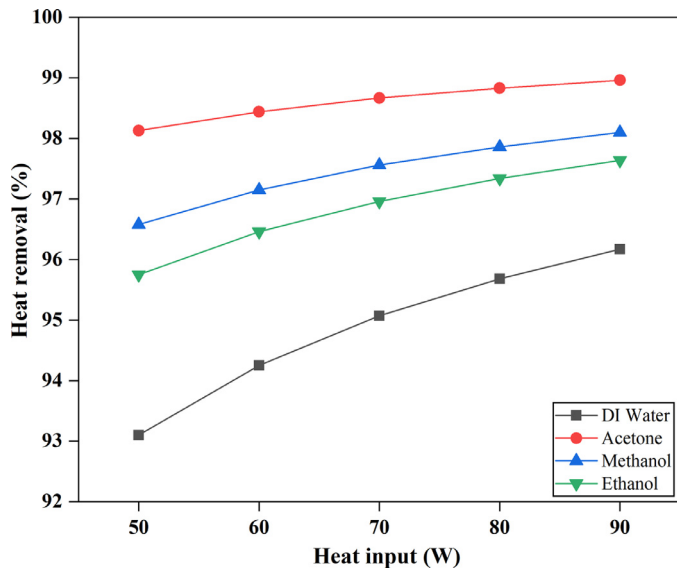


Fig. 7. Enhancement in the percentage of heat removal vs different heat inputs for circulating coolants.

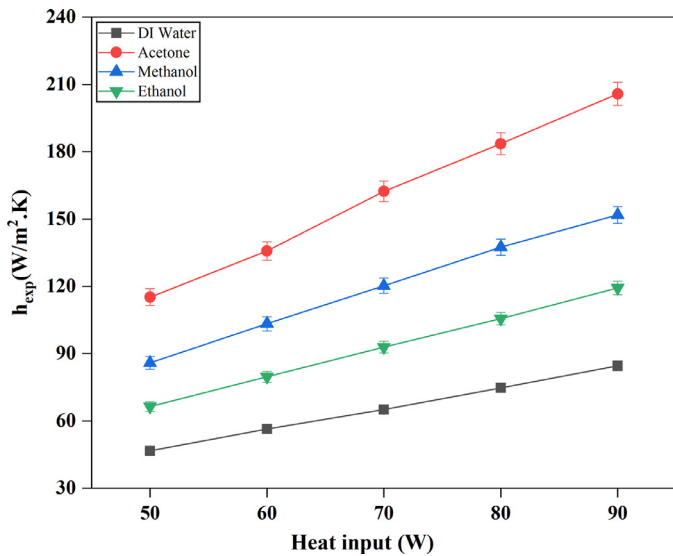


Fig. 8. Increasing rate of heat transfer coefficient with heat inputs for various coolants.

thermal resistance. Fig. 10 illustrates the vapour flow rate of various circulating coolants with the increase of heat input. Since the condensation unit is placed horizontally, the vapour flow rate is high for low latent heat of coolant at maximum heat input and forces the condensate liquid to the coolant tank. This may be the reason for obtaining low thermal resistance. Han et al. [35] reported a low thermal resistance of working fluid at high heat input and low LHV. Also, they found that the viscosity decreases with the rise of heat input that leads to high vapour flow rate. Similar results are reported by Kiatsiriroat et al. [36]. At a higher operating temperature, the nucleate boiling results more amount of superheated vapour leads to low thermal resistance [37]. Therefore, the high vapour flow rate and low LHV are the deciding factors for obtaining the low thermal resistance of acetone.

5.4. Charging performance of PCM

The charging performance is analysed by how fast the steady state temperature of the primary stored PCM is attained and the heat storage

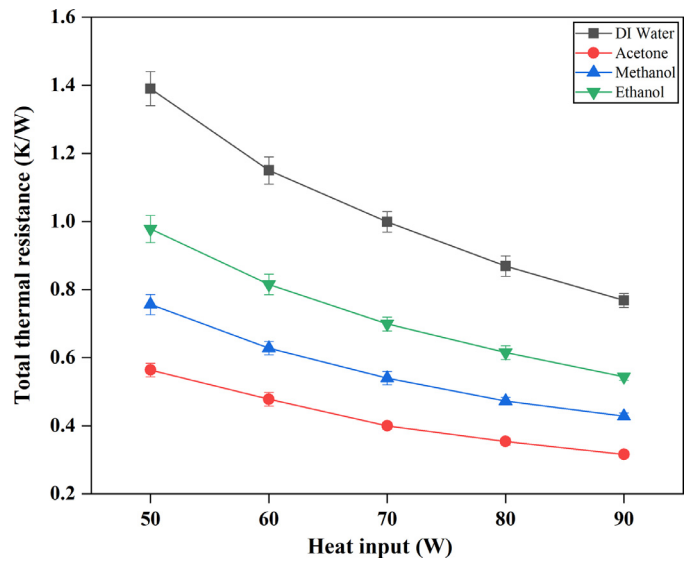


Fig. 9. Effect of heat input on total thermal resistance for various circulating coolants.

capacity by the influence of various circulating coolants. The steady state temperature of PCM is the temperature at which the PCM melts completely thereafter remains constant. In this work, four thermocouples are fixed at a zigzag position in the primary PCM stored annular (Fig. 6) to measure the melting temperature at every 5 min. Fig. 11 represents the temperature variation of PCM at different time intervals for 90 W. It is seen that the vapourized acetone takes 105 min to reach the steady state temperature after that temperature remains same till 200 min. Also, the vapourized methanol, ethanol and DI water take 120, 130 and 160 min respectively after that it maintains the constant temperature. At evaporation section, more amount of heat is generated at maximum heat input. It is then transferred to the primary PCM stored annular which helps to enhance the phase change rate in both circulating coolant and PCM owing to the high temperature difference between PCM and the inside copper tube. Similarly, the time taken to attain the steady state temperature of PCM at different heat inputs over the range of 50 to 80 W is shown in Fig. 12. From the above observations, the PCM can melt congruently and a large amount of heat is extracted from the coolants due to the high vapour flow rate at high

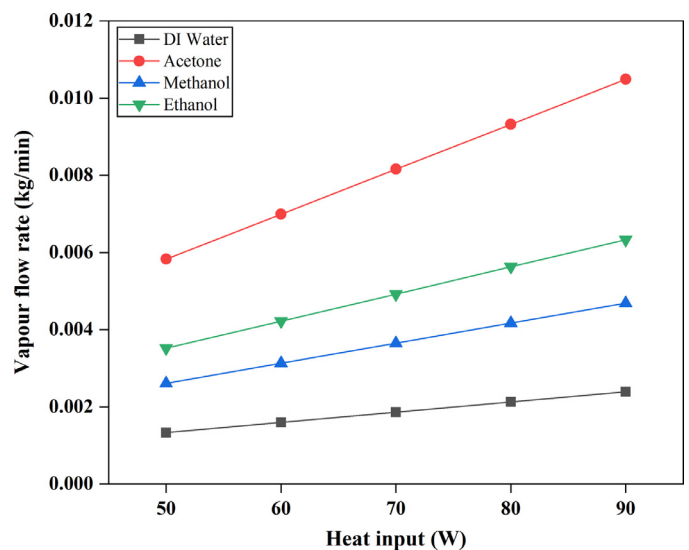


Fig. 10. Increasing rate of vapour flow of different circulating coolants with the effect of heat inputs.

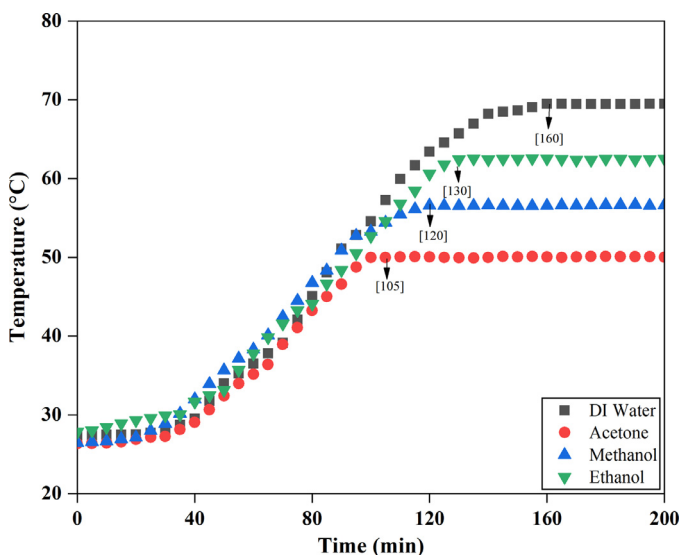


Fig. 11. Temperature variation of PCM by the influence of coolants during charging at 90 W.

Table 4

Thermal power stored in PCM by the influence of coolants.

Circulating coolants	Stored thermal power in PCM (W)				
	50 W	60 W	70 W	80 W	90 W
Acetone	4.16	4.62	4.95	5.62	6.18
DI Water	3.95	4.17	4.40	4.53	4.82
Ethanol	4.05	4.27	4.67	5.18	5.55
Methanol	4.05	4.43	4.91	5.28	5.76

power input. Also, the vapourized acetone takes a shorter time to attain the steady state temperature of the PCM due to the more amount of superheated vapour flow at maximum heat input.

The vapour flow rate of circulating coolant mainly depends on the heat input. Moreover, the velocity of circulating coolants increases with the increase of vapour flow rate resulting in a decrease in thermal resistance. This further causes a high rate of heat transfer between the circulating coolant and PCM. Tiari et al. [38] suggested the heat transfer rate between fluid and the PCM is mainly due to (i) higher rate of convection between the hot fluid and the copper tube and (ii) lower the thermal resistance between heat transfer fluid and the PCM. Similar studies are also reported by Kabaara et al. [26] and Weng et al. [18]. Therefore, the vapour flow rate is the major parameter that affects the

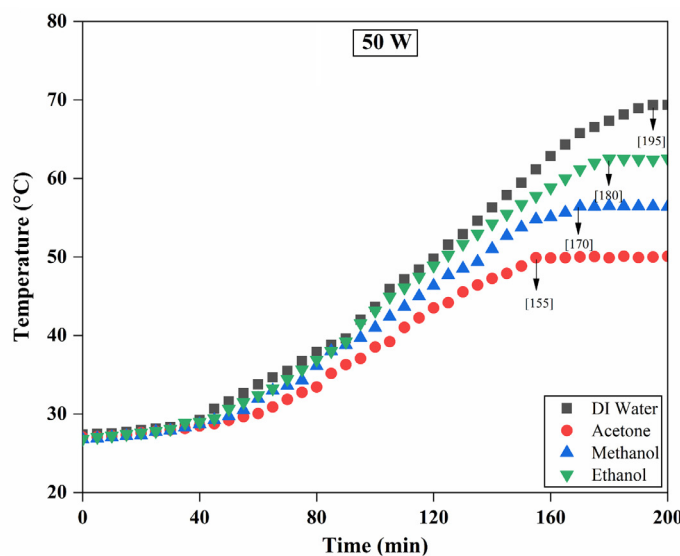
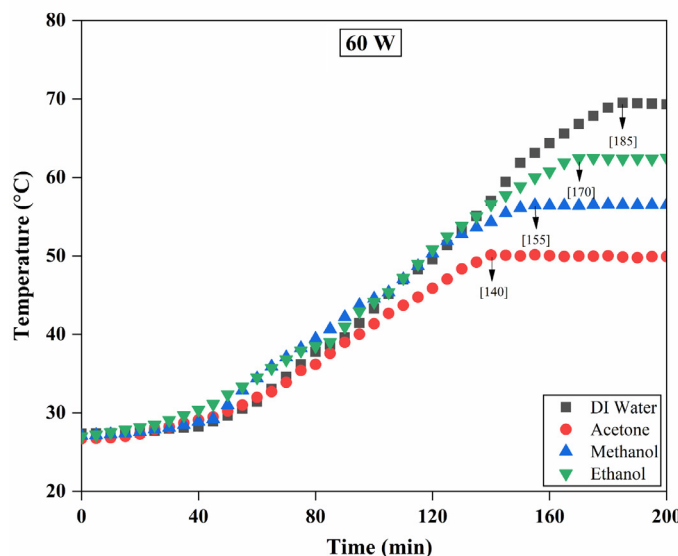
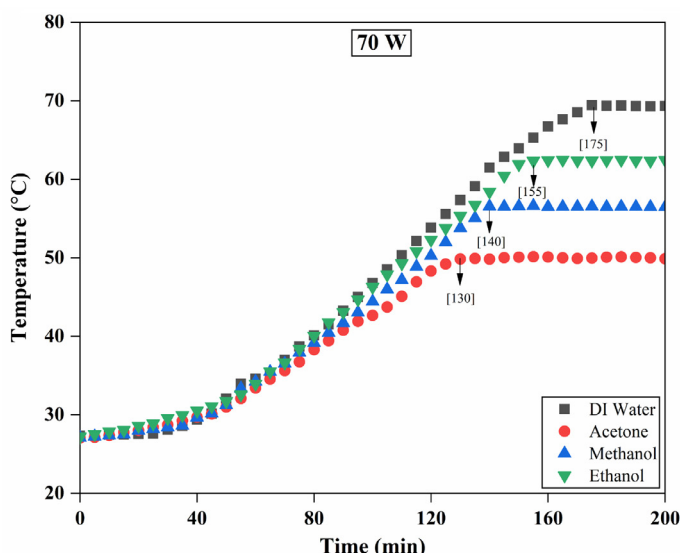
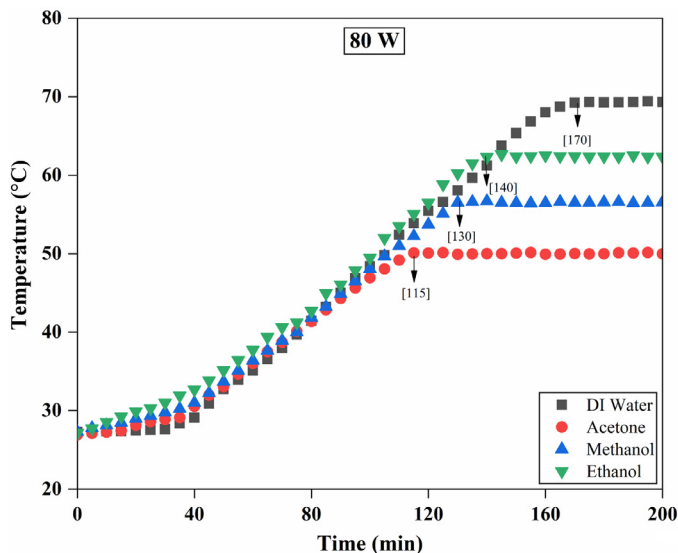


Fig. 12. Temperature of PCM with the time increment in the primary annular during charging when the heat input ranging from 50 to 80 W.

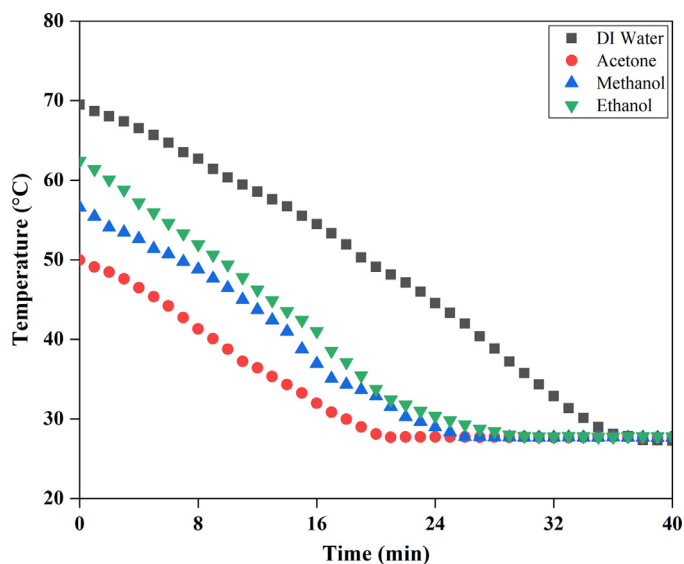


Fig. 13. Temperature variation of PCM during discharging (supplying cold water) at 90 W.

charging performance of PCM. At maximum heat input, the vapour flow rate of the acetone, DI water, methanol and ethanol is obtained as 0.01049, 0.00239, 0.00469 and 0.00633 kg/min respectively (Fig. 10). Also, the vapour flow rate of acetone takes 105 min while DI water takes 160 min to attain the steady state temperature of the melted PCM. The charging rate of vapourized acetone is higher than the other coolants used in this study and an increase of about 34% is found as compared to DI water.

Table 4 represents the stored thermal power in PCM by the influence of various coolants at different heat input. It is seen that the thermal power stored in the PCM increases with the heat input for all circulating coolants. Also, the maximum thermal power absorbed by the PCM is about 6.18 W for vapourized acetone at 90 W due to the high heat carrying capacity, less subcooling effect and less time taken for the complete melting of PCM. Therefore, the maximum amount of stored thermal power by the PCM indicates that a large amount of heat is extracted from the experimental setup.

5.5. Discharging performance of PCM

The discharging performance of PCM is investigated for every 1 min duration. In order to analyse, cold water is allowed to flow through the copper tube during switched OFF condition (Fig. 6). The heat is absorbed due to the temperature difference between PCM and the cold water in the primary PCM stored annular. The outlet valve is closed during this period. At every 1 min, the outlet valve is opened and the temperature of hot water is recorded. This process persists until the PCM becomes solidified. As seen in Fig. 13, the molten PCM resolidifies from 50 to 27.71 °C in 21 min when acetone is used as a circulating coolant whereas DI water, ethanol and methanol resolidifies from 69.5 to 27.82 °C in 37 min, 62.43 to 27.85 °C in 30 min and 56.6 to 27.74 °C in 26 min respectively. Since the time taken is noted to change its phase from molten state to solidification, similar observations are seen for all heat inputs. The steady state temperature of molten PCM is found as low when acetone is used thereby it solidifies at a faster rate during the switched OFF condition of setup. The copper tube is placed at the centre of the primary PCM stored annular. Hence, the heat transfer is a conduction domination process during discharging [22,23]. In general, the rate of heat transfer is faster when the temperature difference between PCM and the inlet cold water is high. However, the complete solidification of PCM takes a long time. For instance, the rate of heat transfer is faster for DI water. But, it takes 37 min to solidify the PCM from molten

state (69.5 °C). Therefore, it is concluded that the molten PCM resolidifies at a faster rate when acetone is used as a circulating coolant.

6. Conclusions

The thermosyphon assisted thermal energy storage system is experimentally investigated for heat dissipation from the electronic devices to maintain optimum performance. The effect of heat input on the percentage of heat removal, HTC and thermal resistance are compared for various circulating coolants. Also, the charging and discharging performance of PCM is analysed by the influence of circulating coolants. The major observations are drawn as follows:

- The maximum percentage of heat removal of acetone is 98.9% at 90 W due to low boiling point and low LHV.
- The HTC increases with the increase of heat input. At the maximum heat input, the acetone has the highest HTC value of about 205.78 W/(m².K) as compared with DI water, ethanol and methanol. It is because of low viscosity and less effect on subcooling.
- At 90 W, the total thermal resistance of DI water, ethanol, methanol and acetone is 0.768, 0.544, 0.428 and 0.316 K/W respectively. It is observed that acetone has low thermal resistance due to high vapour flow rate.
- In the charging process, the vapourized acetone takes 105 min to reach the steady state temperature at maximum heat input after that temperature of PCM remains same. Also, the maximum thermal power absorbed by the PCM is about 6.18 W for vapourized acetone at 90 W owing to high heat carrying capacity and less subcooling effect.
- In discharging, the complete solidification of PCM takes 21 min for acetone as a circulating coolant by virtue of low steady state temperature.

It is suggested that the heat transfer performance of the test facility is more efficient when acetone is used as a circulating coolant during both switched ON and OFF conditions. Also, the above experimental setup is suitable for all the desired range of electronic modules which bring the foolproof thermal management without the use of electricity.

Declaration of Competing Interest

The authors declared that there is no conflict of interest with any individual or organization.

Acknowledgement

The authors would like to thank the Council of Scientific & Industrial Research (CSIR), New Delhi, Government of India for funding this research work (ACK. No.:141202/2K18/1).

References

- M. Janicki, A. Napieralski, Modelling electronic circuit radiation cooling using analytical thermal model, *Microelectronics J.* 31 (2000) 781–785, [https://doi.org/10.1016/S0026-2692\(00\)00059-8](https://doi.org/10.1016/S0026-2692(00)00059-8).
- J. Cao, C. Chen, Y. Su, M.K.H. Leung, M. Bottarelli, G. Pei, Experimental study on the temperature management behaviours of a controllable loop thermosyphon, *Energy Convers. Manag.* 195 (2019) 436–446, <https://doi.org/10.1016/j.enconman.2019.05.031>.
- S.M.S. Murshed, C.A.N. Castro, A critical review of traditional and emerging techniques and fluids for electronics cooling, *Renew. Sustain. Energy Rev.* 78 (2017) 821–833, <https://doi.org/10.1016/j.rser.2017.04.112>.
- M.A. Nazari, M.H. Ahmadi, R. Ghasempour, M.B. Shafii, How to improve the thermal performance of pulsating heat pipes: A review on working fluid, *Renew. Sustain. Energy Rev.* 91 (2018) 630–638, <https://doi.org/10.1016/j.rser.2018.04.042>.
- B. Palm, R. Khodabandeh, Choosing working fluid for two-phase thermosyphon systems for cooling of electronics, *J. Electron. Packag.* 125 (2003) 276–281, [10.1115/1.1571570](https://doi.org/10.1115/1.1571570).
- C. Chang, S. Kuo, M. Ke, S. Chen, two-phase closed-loop thermosyphon for

- electronic cooling, *Exp. heat transf.* 23 (2010) 144–156, <https://doi.org/10.1080/08916150903402807>.
- [7] A.A. Chehade, H. Louahlia-Gualous, S.L. Masson, I. Victor, N. Abouzahab-Damaj, Experimental investigation of thermosyphon loop thermal performance, *Energy Convers. Manag.* 84 (2014) 671–680, <https://doi.org/10.1016/j.enconman.2014.04.092>.
- [8] S. Rittidech, W. Srimuang, Correlation to predict heat-transfer characteristics of a vertical flat thermosyphon (VFT) at normal operating conditions, *Int. J. Heat Mass Transf.* 53 (2010) 5984–5987, [10.1016/j.ijheatmasstransfer.2010.08.011](https://doi.org/10.1016/j.ijheatmasstransfer.2010.08.011).
- [9] W. Srimuang, S. Rittidech, B. Bubphachot, Heat transfer characteristics of a vertical flat thermosyphon (VFT), *J. Mech. Sci. Technol.* 23 (2009) 2548–2554, <https://doi.org/10.1007/s12206-009-0703-y>.
- [10] G.H. Kwon, S.J. Kim, Experimental investigation on the thermal performance of a micro pulsating heat pipe with a dual-diameter channel, *Int. J. Heat Mass Transf.* 89 (2015) 817–828, <https://doi.org/10.1016/j.ijheatmasstransfer.2015.05.091>.
- [11] F. Cataldo, J.R. Thome, Experimental performance of a completely passive thermosyphon cooling system rejecting heat by natural convection using the working fluids R1234ze, R1234yf and R134a, *J. Electron. Packag.* 140 (2018) 021002, <https://doi.org/10.1115/1.4039706>.
- [12] T. Tsai, H. Wu, C. Chang, S. Chen, Two-phase closed thermosyphon vapor-chamber system for electronic cooling, *Int. Commun. Heat Mass Transf.* 37 (2010) 484–489, <https://doi.org/10.1016/j.icheatmasstransfer.2010.01.010>.
- [13] T. Hao, H. Ma, X. Ma, Heat transfer performance of polytetrafluoroethylene oscillating heat pipe with water, ethanol, and acetone as working fluids, *Int. J. Heat Mass Transf.* 131 (2019) 109–120, <https://doi.org/10.1016/j.ijheatmasstransfer.2018.08.133>.
- [14] L.N. Narasimhan, Assessment of latent heat thermal storage systems operating with multiple phase change materials, *J. Energy Storage* 23 (2019) 442–455, <https://doi.org/10.1016/j.est.2019.04.008>.
- [15] H. Nazir, M. Batool, F.J.B. Osorio, M. Isaza-Ruiz, X. Xu, K. Vignarooban, P. Phelan, A.M. Inamuddin, Kannan, recent developments in phase change materials for energy storage applications: A review, *Int. J. Heat Mass Transf.* 129 (2019) 491–523, <https://doi.org/10.1016/j.ijheatmasstransfer.2018.09.126>.
- [16] L. Kalapala, J.K. Devanuri, Influence of operational and design parameters on the performance of a PCM based heat exchanger for thermal energy storage – A review, *J. Energy Storage* 20 (2018) 497–519, <https://doi.org/10.1016/j.est.2018.10.024>.
- [17] B.P. Walsh, S.N. Murray, D.T.J. O'Sullivan, Free-cooling thermal energy storage using phase change materials in an evaporative cooling system, *Appl. Therm. Eng.* 59 (2013) 618–626, <https://doi.org/10.1016/j.applthermaleng.2013.06.008>.
- [18] Y. Weng, H. Cho, C. Chang, S. Chen, Heat pipe with PCM for electronic cooling, *Appl. Energy*. 88 (2011) 1825–1833, <https://doi.org/10.1016/j.apenergy.2010.12.004>.
- [19] E.M. Alawadhi, C.H. Amon, PCM thermal control unit for portable electronic devices: experimental and numerical studies, *IEEE Trans. Components Packag. Technol.* 26 (2003) 116–125, <https://doi.org/10.1109/TCAPT.2003.811480>.
- [20] L. Fan, Y. Xiao, Y. Zeng, X. Fang, X. Wang, X. Xu, Z. Yu, R. Hong, Y. Hu, K. Cen, Effects of melting temperature and the presence of internal fins on the performance of a phase change material (PCM)-based heat sink, *Int. J. Therm. Sci.* 70 (2013) 114–126, <https://doi.org/10.1016/j.ijthermalsci.2013.03.015>.
- [21] B. Hu, Q. Wang, Z. Liu, Fundamental research on the gravity assisted heat pipe thermal storage unit (GAHP-TSU) with porous phase change materials (PCMs) for medium temperature applications, *Energy Convers. Manag.* 89 (2015) 376–386, <https://doi.org/10.1016/j.enconman.2014.10.017>.
- [22] Y.H. Diao, S. Wang, C.Z. Li, Y.H. Zhao, T.T. Zhu, Experimental study on the heat transfer characteristics of a new type flat micro heat pipe heat exchanger with latent heat thermal energy storage, *Exp. Heat Transf.* 30 (2017) 91–111, <https://doi.org/10.1080/08916152.2016.1179355>.
- [23] G. Chen, N. Li, H. Xiang, F. Li, Experimental study on thermal characteristics of finned coil lhu using paraffin as phase change material, *J. Heat Transf.* 139 (2017) 042901, <https://doi.org/10.1115/1.4035321>.
- [24] H. Behi, M. Ghanbarpour, M. Behi, Investigation of PCM-assisted heat pipe for electronic cooling, *Appl. Therm. Eng.* 127 (2017) 1132–1142, [10.1016/j.applthermaleng.2017.08.109](https://doi.org/10.1016/j.applthermaleng.2017.08.109).
- [25] <http://ddbonline.ddbst.de>.
- [26] M. Kabbara, D. Groulx, A. Joseph, Experimental investigations of a latent heat energy storage unit using finned tubes, *Appl. Therm. Eng.* 101 (2016) 601–611, <https://doi.org/10.1016/j.applthermaleng.2015.12.080>.
- [27] C. Yadav, R.R. Sahoo, Exergy and energy comparison of organic phase change materials based thermal energy storage system integrated with engine exhaust, *J. Energy Storage* 24 (2019) 100773, <https://doi.org/10.1016/j.est.2019.100773>.
- [28] Y. Feng, R. Wei, Z. Huang, X. Zhang, G. Wang, Thermal properties of lauric acid filled in carbon nanotubes as shape-stabilized phase change materials, *Phys. Chem. Chem. Phys.* 20 (2018) 7772–7780, <https://doi.org/10.1039/c7cp08557e>.
- [29] X. Fu, Z. Liu, Y. Xiao, J. Wang, J. Lei, Preparation and properties of lauric acid/diatomite composites as novel form-stable phase change materials for thermal energy storage, *Energy Build* 104 (2015) 244–249, <https://doi.org/10.1016/j.enbuild.2015.06.059>.
- [30] A. Sari, A. Karaipekli, C. Alkan, Preparation, characterization and thermal properties of lauric acid/expanded perlite as novel form-stable composite phase change material, *Chem. Eng. J.* 155 (2009) 899–904, <https://doi.org/10.1016/j.cej.2009.09.005>.
- [31] J.P. Holman, *Experimental Methods for Engineers*, 7th edn, McGraw-Hill, New York, 2001 Chapter 3.
- [32] X. Cui, Y. Zhu, Z. Li, S. Shun, Combination study of operation characteristics and heat transfer mechanism for pulsating heat pipe, *Appl. Therm. Eng.* 65 (2014) 394–402, <https://doi.org/10.1016/j.applthermaleng.2014.01.030>.
- [33] S. Shi, X. Cui, H. Han, J. Weng, Z. Li, A study of the heat transfer performance of a pulsating heat pipe with ethanol-based mixtures, *Appl. Therm. Eng.* 102 (2016) 1219–1227, <https://doi.org/10.1016/j.applthermaleng.2016.04.014>.
- [34] R. Senjaya, T. Inoue, Bubble generation in oscillating heat pipe, *Appl. Therm. Eng.* 60 (2013) 251–255, <https://doi.org/10.1016/j.applthermaleng.2013.06.041>.
- [35] H. Han, X. Cui, Y. Zhu, S. Sun, A comparative study of the behavior of working fluids and their properties on the performance of pulsating heat pipes (PHP), *Int. J. Therm. Sci.* 82 (2014) 138–147, <https://doi.org/10.1016/j.ijthermalsci.2014.04.003>.
- [36] T. Kiatsiriroat, A. Nuntaphan, J. Tiansuwan, Thermal performance enhancement of thermosyphon heat pipe with binary working fluids, *Exp. Heat Transf.* 13 (2000) 137–152, <https://doi.org/10.1080/089161500269517>.
- [37] R. Naik, V. Varadarajan, G. Pundarikka, K.R. Narasimha, Experimental investigation and performance evaluation of a closed loop pulsating heat pipe, *J. Appl. Fluid Mech.* 6 (2013) 267–275.
- [38] S. Tiari, M. Mahdavi, S. Qiu, Experimental study of a latent heat thermal energy storage system assisted by a heat pipe network, *Energy Convers. Manag.* 153 (2017) 362–373, <https://doi.org/10.1016/j.enconman.2017.10.019>.